J. Eng. Technol. Sci., Vol. 53, No. 5, 2021, 210511

Metal-supported SOFC Fabricated by Tape Casting and Its Characterization: A Study of the Co-sintering Process

Zaka Ruhma[1,2,3], Keiji Yashiro[1], Itaru Oikawa[4], Hitoshi Takamura[4] & Tatsuya Kawada[1,*]

[1]Graduate School of Environmental Studies, Tohoku University, 6-6-01 Aoba, Aramaki, Aoba-ku, Sendai, 980-8579 Japan
[2]Ship Machinery Study Programme, Faculty of Vocational Studies, Indonesia Defense University, Jalan Ki Hajar Dewantara, Belu Regency, 85752 Indonesia
[3]Center for Defense and Security Technology, Institut Teknologi Bandung, Jalan Ganesha 10, Bandung, 40132 Indonesia
[4]Graduate School of Engineering, Tohoku University, 6-6-02 Aoba, Aramaki, Aoba-ku, Sendai, 980-8579 Japan
*E-mail: kawada@ee.mech.tohoku.ac.jp

Highlights:

- Reporting the effect of the variation of the amount of pore former added to the metallic layer on cell curvature.
- Reporting the effect of a lid on top of the cell during sintering.
- Reporting the residual stresses resulted from the change of curvature after sintering.
- Reporting that the permeability of the metal is important for H_2 gas feeding for the cell to function.
- Reporting that a single half-cell with 5.5 g of pore former in the stainless steel layer sintered at 1300 °C for 5 minutes was able to produce 10 mW/cm^2 on 10%H_2-Ar/3%H_2O as fuel and air as oxidant.

Abstract. Metal-supported SOFC consists of metallic and ceramic multilayers. Since the cell has to be flat, interaction between the layers that results in a flat sintered layer needs to be studied. The method used here was changing the starting materials through several experiments. Here, we highlight the effects of pore former in metal slurry on the sintered half-cell multilayer of a 430L metallic support, an NiO-8YSZ anode, and an 8YSZ electrolyte. The results show that by changing the amount of pore former in the 430L metal slurry changed the sinterability of the metal layer. This change of the sinterability of the metal support affected the final warpage state of the cell. This study aid in explaining the sintering phenomena between layers of metal-supported SOFCs.

Keywords: *ceramic processing; co-sintering; MS-SOFC; residual stress; tape casting.*

1 Introduction

After the previous successful anode-supported SOFCs, metal-supported solid oxide fuel cells (MS-SOFCs) are currently developed to endure more severe

Received April 16th, 2021, August 13th, 2021, Accepted for publication August 31st, 2021.
 ISSN: 2337-5779, DOI: 10.5614/j.eng.technol.sci.2021.53.5.11

environments under various mechanical stress and redox phenomena during SOFC operation. In MS-SOFCs, porous metal is put under the functional anode or above the cathode, acting not only as mechanical support but also as current collector. They also show better thermal and electrical conductivity compared to all-ceramic fuel cells, thus resulting in better redox stability, which creates more uniformity when undergoing surface oxidation [1].

Several methods can be used to fabricate multilayered MS-SOFCs. Based on the preparation and the particle deposition process, deposition methods for MS-SOFC fabrication can be classified into wet ceramic sintering and physical deposition. Examples of wet ceramic sintering methods to fabricate MS-SOFCs can be found in the early work of Villareal, *et al.* on Fe-Cr, NiO-YSZ, YSZ multilayers [2] and in the work of Zhou, *et al.* on the infiltrated electrode design of MS-SOFCs [3]. As for the physical deposition method, examples can be seen in the work of Hwang, *et al.* [4] on the use of atmospheric plasma spraying (APS) and in the work of Ju, *et al.* [5] on the use of pulsed laser deposition (PLD). In comparison to wet ceramic sintering, the physical method suffers from several demerits, such as high vacuum chamber requirement, uneven deposition for large samples, and high cost. As for APS, the electrolyte thickness has to be more than 50 micron and micro-crack formation in the post-annealing process can cause problems.

By using the route of wet ceramic sintering, it is possible to obtain a thin film with a good microstructure, while involving simpler operation. However, the sintering process requires compatibility between all layers composing the cell. The electrolyte and electrode designs of the cell can often be highly unsymmetrical, which makes it difficult to obtain a cell without warpage after sintering at high temperature.

The metal support and the electrodes can have degrading interaction, such as Fe-Cr interaction with an Ni-based anode [6] and Cr poisoning of the cathode materials [1]. To obtain a flat cell, the electrolyte and electrode designs can be made symmetrical by employing symmetrical thick infiltrated electrodes, such as a symmetrical metal backbone [7] and thick symmetrical metal and YSZ electrodes [3]. In order to prevent degrading interaction between the metal and the electrodes, diffusion barrier layers (DBLs) are used [6]. However, due to the preference of a symmetrical structure for wet ceramic sintering, DBLs can almost only be applied via the physical deposition route. By studying the details of sintering phenomena in wet ceramic processing, specifically the tape-casting sintering process, we aimed to obtain a flat cell with asymmetrical metal support, electrolyte, and electrode designs. In this work, we investigated the sintering phenomena of a 430L stainless steel metal support, an NiO-YSZ anode, and an 8

mol% YSZ electrolyte half-cell. The cathode was sintered in-situ during cell testing. In a future work, DBL will be added to the half-cell.

2 Experimental

2.1 Outline of Fabrication

In preparing the MS-SOFC, a tape-casting machine, also called doctor blade, was used. Ceramic/metal powder was mixed with selected organic solvents (isopropanol and toluene), a polyvinyl butyral binder, a propylene glycol dispersant, and a polyoxyethylene (10)-octylphenyl ether foam remover. To customize the porosity of the support and the electrode layers an acrylic polymer pore former (BMX-5, Sekisui Plastics) with a size of about 5 micron was added. During co-sintering, shrinkage matching for all layers should be considered carefully to achieve less constrained sintering.

2.2 Tape-casting Procedure

Layered sheets of 430L stainless steel (Osprey Sandvik 20 µm-45 µm), NiO-F (Sumitomo Metal Mining Japan) 8 mol% YSZ, and 8 mol% YSZ (Tosoh Japan) were made. The layers were tape-casted on top each other after drying one layer. In this work, 100%H_2 was used during sintering. Tables 1 to 3 show the tape-casting recipes used in this work. The slurry components were mixed together in a planetary ball mill for 3 hours at 300 rpm, followed by removing bubbles in a vacuum container. To prevent metal deformation during milling, an exception in metal slurry mixing, one ball of 1 cm in size was used during milling. The blade gap for the stainless steel, NiO-YSZ, and YSZ slurries was about 900 micron, 600 micron, and 850 micron, respectively, where the stainless steel slurry was tape-casted first.

Table 1 Tape casting recipe of stainless steel layer.

Quantity	Material
35 g	Stainless steel
Variation of 3.7, 4, 4.5, 5, 5.5, 6, and 7 g	Acrylic
5.6 g	Polyvinyl butyral
8.3 mL	Isopropanol
14 mL	Toluene
5.1 mL	Dibuthyl phthalate
0.45 mL	Mariarim AKM-0531
0.45 mL	Polyoxyethylene (10)-octylphenyl ether

Table 2 Tape-casting recipe of stainless steel layer.

Quantity	Material
11.9 g	NiO
6.5 g	YSZ
2.2 mL	Polyvinyl butyral
6 mL	Isopropanol
6 mL	Toluene
1.7 mL	Dibuthyl phthalate
0.4 mL	Propylene glycol
0.4 mL	Polyoxyethylene (10)-octylphenyl ether

Table 3 Tape-casting recipe of stainless steel layer.

Quantity	Material
15.2 g	YSZ
1.7 g	Polyvinyl butyral
3.75 mL	Isopropanol
7.5 mL	Toluene
1.8 mL	Dibuthyl phthalate
0.3 mL	Propylene glycol
0.3 mL	Polyoxyethylene (10)-octylphenyl ether

2.3 Co-sintering Process

The half cells were sintered in a tube furnace at 1300 °C with the holding time varied at 5 minutes, 3 hours, and 5 hours in a 100%H_2 atmosphere with heating rate and cooling rate of 1 °C per min. The 100%H_2 atmosphere was kept by flowing H_2 gas at a flowrate of 100 ccm. During the debinding process, an air atmosphere was used with the holding time varied at 250 °C, 300 °C, 350 °C, and 400 °C for 1 hour each, and finally at 450 °C for 6 hours to ensure the removal of organics. Alumina plate was used as the substrate to place the half-cell on. The metal surface was placed upwards to prevent metal and alumina interdiffusion.

2.4 Electrochemical Measurement

For electrochemical measurement, a single fuel cell was sealed using vermiculite sealing (Thermiculite 866, Flexitalic Group) in an all-ceramic SOFC Test Holder (Chino Japan). Silver paste was applied to the half-cell as cathode. Pt meshes were used as current collectors of both the cathode and the anode side. Current-voltage curves were obtained using a Zahner Zennium Electrochemical Workstation (Zahner Germany) at 600-700 °C with the cathode exposed to air

and the anode to humidified (3% H_2O) hydrogen. The active area of the single cell was 0.45 cm^2.

2.5 Characterization

In order to explain the reason behind the difference in multilayer warpage behavior after sintering, microstructure observation and residual stress measurements were done. The surface and cross-section microstructure of the 8 mol% YSZ and the stainless steel were observed by scanning electron microscope (SEM). The residual stresses of the layers were measured by μ-X360s Portable X-ray Residual Stress Analyzer (Pulstec, Japan) using a collimator size of 1 mm on the half-cell surface of the stainless steel and the 8 mol% YSZ.

3 Results and Discussion

3.1 Effect of Pore Formers on Co-sintering

The half-cells in Figure 1 were sintered at 1300 °C for a holding time of 5 minutes. Interestingly, it could be seen that the amount of pore former added to the stainless steel slurry affected the sinterability of the stainless steel layer, thus changing the multilayer final warpage direction.

Figure 1 Metal-supported half-cell (stainless steel, NiO-YSZ, and YSZ) sintered with amount of pore former added varied at 7 g, 6 g, 5.5 g, 5 g, and 4 g, from right to left, as described before in tables 1 to 3 with tape-casting recipes for a sintering time of 5 minutes at 1300 °C.

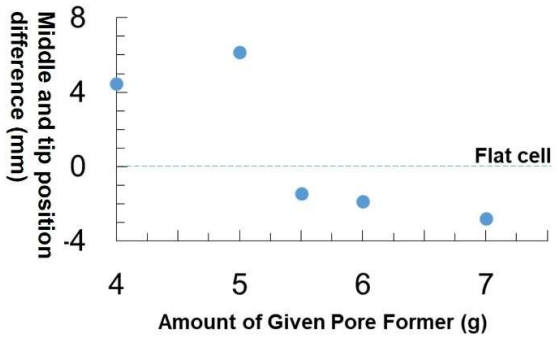

Figure 2 Quantification of warpage of the half-cell sintered at 1300 °C for 5 minutes plotted along with the various amounts of pore former added.

3.2 Effect of Alumina Plate Lid

The first trials were done with half-cells put on an alumina plate in open space with the stainless steel face on top to prevent Fe-Cr interdiffusion with alumina. Figure 3 shows the result of a half-cell that was put on an alumina plate sandwiched with a spacer of about 2 mm to create a lid to homogenize the temperature of the half-cell. The half-cell with 4.5 g of pore former, as shown in Figure 3, had a flat appearance in the second trial under the same sintering condition of 1300 °C and a holding time of 5 minutes. The half-cell with 5.5 g of pore former cracked when a lid was added, as opposed to good flatness when it was sintered in open space.

Figure 3 Metal-supported half-cell (SS, NiO-YSZ, and YSZ) sintered with different amounts of pore former but with an alumina lid with a space of 2 mm compared to the half-cells in Figure 1, which were sintered in open space without a lid.

3.3 Effect of Sintering Time

A short sintering time may leave the pores due to the lack of grain growth, which helps pore closure during sintering. In the next trials we increased the sintering time to 3 h and 5 h, as shown in Figures 4 and 5, respectively. The increased sintering time of 3 h led to a higher increase of stainless steel sinterability compared to the sinterability of the 8 mol% YSZ. Figure 4 shows that the stainless steel with 5.5 g of pore former had warpage on the stainless steel side. The warpage can be solved by decreasing the amount of pore former to 4 g and adding a lid with a spacer to homogenize the temperature.

Figure 4 Metal-supported half-cell (SS, NiO-YSZ, and YSZ) sintered with amount of pore former added varied at 4 g, 4 g, 5.5 g, from right to left, as described before in tables 1 to 3 with tape casting recipes, for a prolonged sintering time of 3 h at 1300 °C, where the half-cell with 4 g of pore former in the middle picture has a lid with a space of 2 mm from the surface.

Figure 5 shows that decreasing the amount of pore former to 3.7 g to be sintered at a prolonged time of 5 h in open space can solve the warpage problem due to the increased sinterability of the stainless steel. However, at a lower pore former content of 3.7 g, the stainless steel slurry was unstable and quickly sedimented. The authors experienced reproducibility difficulties with the half-cell with 3.7 g of pore former and a sintering time of 5 hours at 1300 °C. Increasing the amount of binder from a point of origin of 5.6 g to 7 g may aid the stability of the slurry, but it was observed that the metal warping then severely increased.

Figure 5 Metal-supported half-cell coated with carbon coating (stainless steel, NiO-YSZ, and YSZ) sintered with 3.7 g of pore former as described before in table 1 to 3 with tape-casting recipes, for a prolonged sintering time of 5 h at 1300 °C in open space.

3.4 Microstructures

Microstructure observations by SEM of all samples are shown in Figures 6-15. The grain size of the 8 mol% YSZ with a sintering time of 5 min was on average far below 1 µm due to a lack of grain growth. As the sintering process proceeds, the grain size increases due to grain growth. The same happens with stainless steel particles: the dihedral angle between the particles becomes larger and even diminishes, as can be seen in Figure 10.

The purpose of this study was to compare the different states of the samples during sintering with different amounts of pore former added and the same sintering holding time. However, making a morphology comparison of a three-dimensional surface is difficult when both are almost the same in microstructure. Further study of the cross-sectioned two-dimensional structure was made, as shown on Figure 12-15. In order to quantify the porosity of the surface by using cross-section microstructure images, dot analysis was used to statistically quantify the surface porosity, where the porosity of the surface had a maximum analyzed porosity depth of about 80 µm, i.e. two stainless steel particles. The red dots represent the porosity while the blue dots represent dense parts. It can be seen in Figure 16 that the surface porosity of the support changed with sintering condition. For the sample sintered in open space at 1300 °C for 5 min it can be seen that more pore former added to the stainless steel layer resulted in more porosity of the stainless steel until reaching the maximum surface porosity at 5.5

g of pore former, after which the porosity decreased slightly when more former was added.

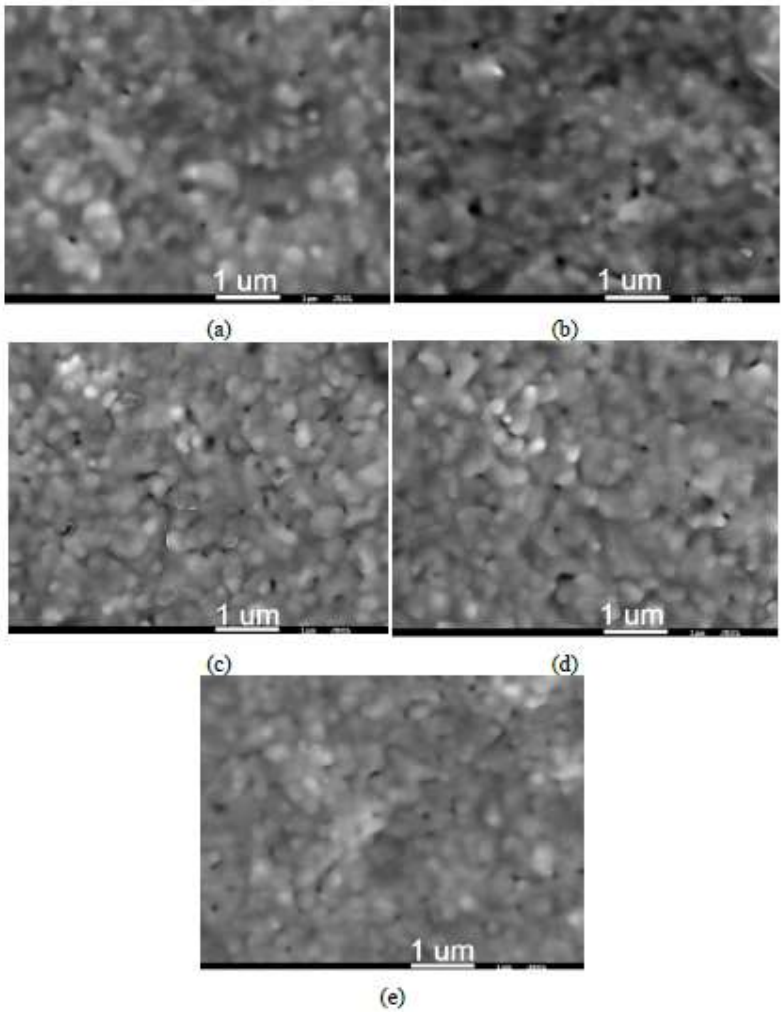

Figure 6 Surface microstructure of the 8 mol% YSZ sintered at 1300 °C for 5 minutes: (a) half-cell with 7 g of pore former in the stainless steel, (b) containing 6 g of pore former, (c) containing 5.5 g of pore former, (d) containing 5 g of pore former, (e) containing 4 g of pore former.

This result shows that the 5.5-g pore former sample that had the best flatness also had the maximum surface porosity among the sintered samples at the same

sintering conditions. However, when the bulk stainless porosity was observed, the 5.5-g pore former sample gave a decrease in bulk porosity from the local maximum of the 5-g pore former sample, after which it decreased when more pore former was added and finally reached its new maximum bulk porosity, as shown in Figure 17 for the sample with 7 g of pore former sintered at 1300 °C for 5 minutes. The cause is unclear, but it is speculated that this is due to the cell's overall curvature (slightly flat) contributing to its particle and pore arrangement to favor about the same distribution of pores on the bulk and surface of the metallic layer.

When a lid was provided with the initial purpose of making the temperature more uniform during sintering, it was found that for the sample with 4.5 g of pore former this resulted in oversintering of the stainless steel, so the surface porosity was very low, as can be seen in Figure 16. Even though the surface porosity of this sample was low, it had the highest bulk porosity among the sintered samples with the same sintering conditions, as shown in Figure 17. It is thought that pore coalescence and pore migration from the surface was the cause of the higher bulk porosity of the samples sintered with an alumina plate lid. Comparing the sintered sample for 5 minutes, 3 h, and 5 h of sintering, it was found that prolonging the sintering time had the same resulting tendency as providing a lid without prolonged sintering time. As shown in Figure 16, prolonging the sintering time to 3 h, the surface porosity of the sample with 5.5 g of pore former was decreased significantly, from 26% to 2.3%. However, it can be seen in Figure 17 that further prolonging the sintering time and addition of more pore former increases the surface porosity. This can be explained by the end-stage sintering condition, indicated by a decrease of interparticle neck growth between the stainless particles, which promotes small pore closure and pore migration and leads to larger pores due to coalescence in bulk stainless steel and a new pore structure of the surface.

Other reported works on constrained sintering of half-cells without interlayer can be found in Refs. Villarreal, *et al.* [2] and Zhou, *et al.* [8], with neither of them providing information about the camber characteristics of the cell. No full metal structure of their half-cells are shown; a maximum of 100 μm of the metallic layers is shown. As for the work of Zhou, *et al.* [8], it seemed that the metal particles were deformed with a size in the range of 10-20 μm. This deformation may have occurred during the milling process or slurry preparation. As for the work of Villareal, *et al.* [2], the irregular metal particles showed a wide particle size range, from 10 μm to 40 μm and the particles were loosely sintered, indicating low particle packing before sintering. The method that was used to loosen the metal particles after sintering is not mentioned. Considering the temperature of 1350 °C for 4 h in the work of Villareal, *et al.*[2], the metal particles should have been sintered close to fully-dense when good particle

packing was the condition of the green layers before sintering. However, the work showed that the layer was loosely packed after sintering, with large pore sizes compared to the particle agglomeration size. In order to understand the actual phenomena that occur during the sintering of this multilayer, experience in doing this kind of sintering is needed. However, the full structure of the cell and information on the camber characteristics are not provided.

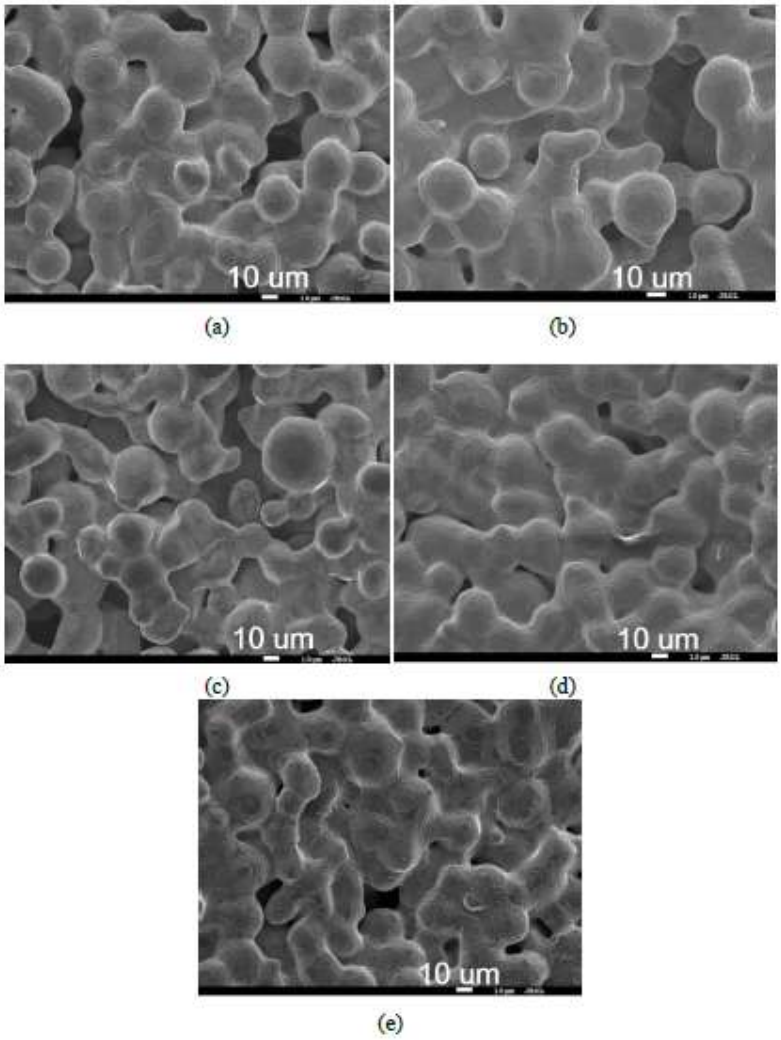

Figure 7 Surface microstructure of the 430L stainless steel sintered at 1300 °C for 5 minutes: (a) a half-cell with 7 g of pore former to the stainless steel, (b)

containing 6 g of pore former, (c) containing 5.5 g of pore former, (d) containing 5 g of pore former, (e) containing 4 g of pore former.

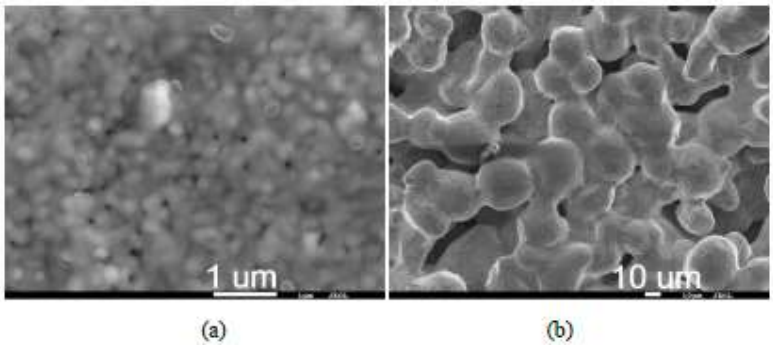

Figure 8 Microstructure of the half-cell with 4.5 g of pore former in the stainless steel sintered with an alumina plate lid spaced by 2 mm at 1300 °C for 5 minutes: (a) the 8 mol% YSZ surface, (b) the stainless steel surface.

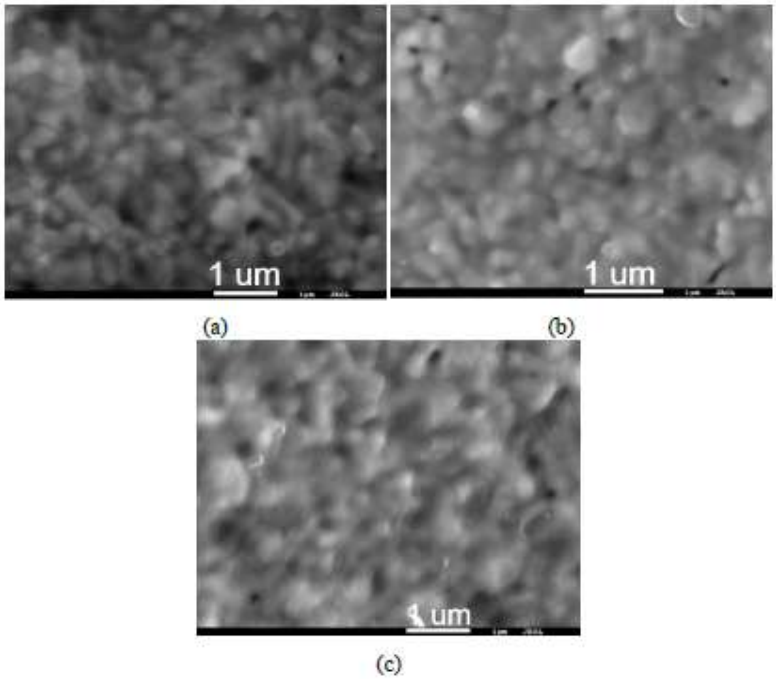

Figure 9 Surface microstructure of the 8 mol% YSZ sintered at 1300 °C for 3 hours: (a) half-cell with 4 g of pore former in the stainless steel sintered in open

space, (b) containing 4 g of pore former, sintered with an alumina plate lid spaced by 2 mm, (c) containing 5.5 g of pore former sintered in open space.

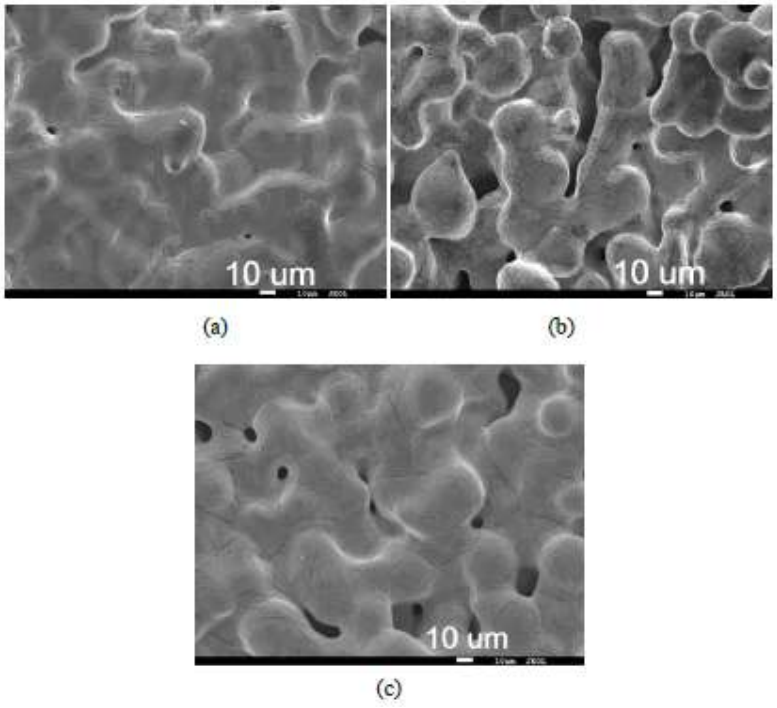

Figure 10 Surface microstructure of the 430L stainless steel sintered at 1300 °C for 3 hours: (a) half-cell with 4 g of pore former in the stainless steel sintered in open space, (b) containing 4 g of pore former sintered with an alumina plate lid spaced by 2 mm, (c) containing 5.5 g of pore former sintered in open space.

Another work on co-sintering of unsymmetrical cells is Toor, *et al.* [9]. By using an intermediate layer of SS-YSZ, they expected to obtain a flat layer. However, they were not able to obtain a flat sample with variation of the number of intermediate layers. No information is provided on changes in the camber characteristics with variation of the number of intermediate layers. A flat half-cell was reported to be obtainable by adding 0.5 $g.cm^{-2}$ to the half-cell. However, the burn-out of the binder seemed to be incomplete, as the 8YSZ color was black. By infiltration of NiO/SDC at the anode and a screen-printed LSCF/GDC cathode, the cell produced a low power density of 0.66 $mW.cm^{-2}$, which may be related to incomplete binder burn-out during processing.

As for the theoretical derivation of this kind of sintering phenomena, it can be highly complicated. Green, *et al.* [10] considered how powder packing evolves from wet ceramic processing. For instance, everything from the tape-casting process to the sintering process needs to be known for a proper simulation. This means that the experimentalist needs to provide details of the green body (pore size distribution, grain size distribution, distribution of defects) as a function of process technology and density to provide a proper simulation [10]. For instance, measuring density gradients in the green specimen can be done by X-ray microtomography. It has further been reported that discrete element simulations can be done from observed microstructures by X-ray microtomography [11].

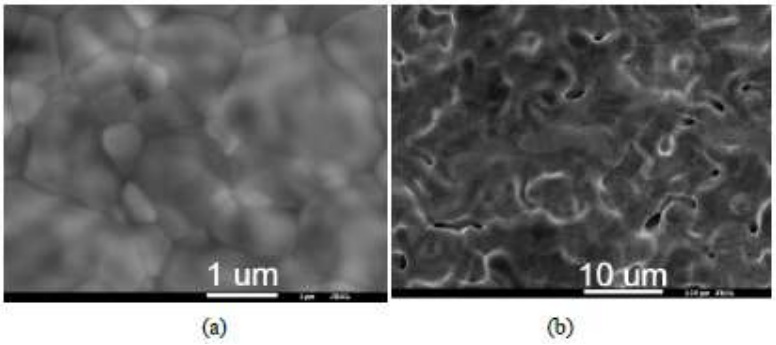

Figure 11 Microstructure of the half-cell with 3.7 g of pore former in the stainless steel sintered in open space at 1300 °C for 5 hours: (a) 8 mol% YSZ surface, (b) stainless steel surface.

Using the discrete element method in SOFC applications that simulate the addition of pore former to free-standing NiO-YSZ (including its reduction into Ni-YSZ) and a bilayer of LSM/LSM+YSZ showed that the simulations in [12] were unable to give the resulting warpage caused by sintering mismatch. Interestingly, the pore former effects in the discrete element method can be varied in its agglomeration state. Other alternative simulations to understand the experimental result can de done by using the densification based finite element method (DFEM) [13,14]. Different from the discrete element method (DEM), [12], DFEM is able to image the resulted curvature during sintering by using several material parameters obtained experimentally. However, DFEM is unable to give information about microstructural evolution [15]. DEM can be coupled with DFEM to model the initial stage of sintering with DFEM. However, DEM alone is not able to fully cover all microstructure evolution phenomena during the whole sintering path. In order to be able to cover all microstructure evolution phenomena during sintering, a kinetic Monte Carlo (KMC) simulation is needed [15]. From Lu, *et al.* [16] it is also known that two structures with the same YSZ

material but with different porosity cause mismatch stress, which will lead to layer curvature. To make the simulation more meaningful, DFEM can be coupled with DEM during the initial stage of sintering, and coupled with KMC during the later stages of sintering. By understanding the sintering phenomena in detail, several strategies can be used to make MS-SOFCs and simulation proposals, for their processing is still open.

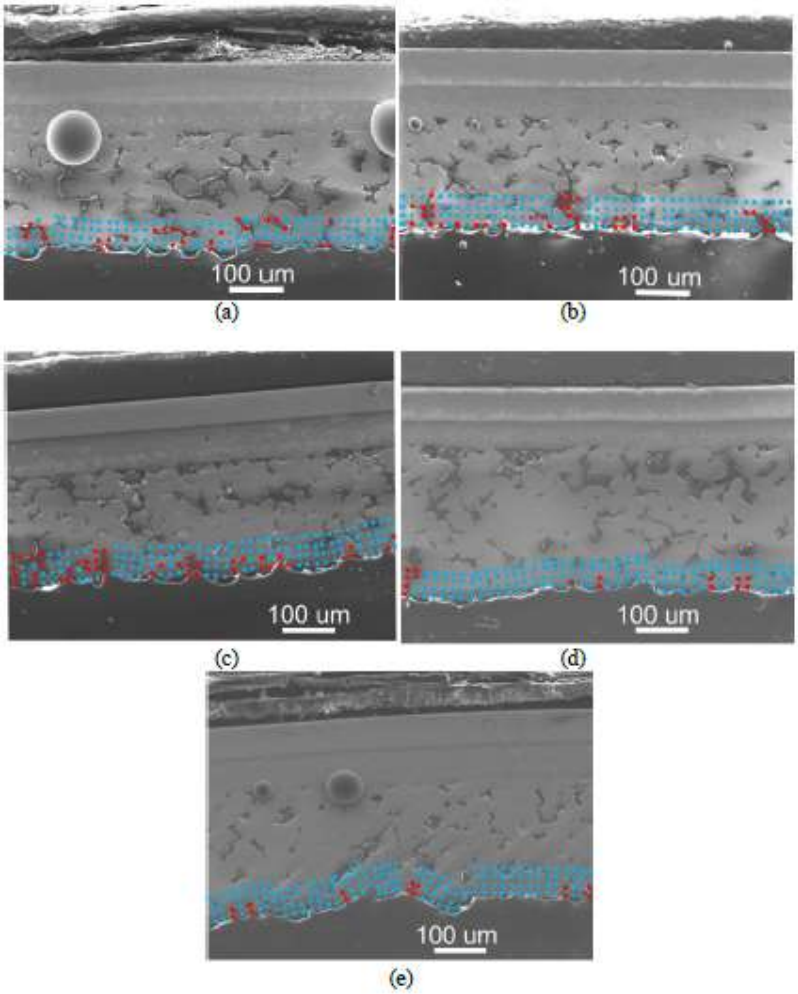

Figure 12 Cross-section of the microstructure of half-cells sintered at 1300 °C for 5 minutes in open space with variation of amount of pore former in the stainless steel: (a) 7 g, (b) 6 g, (c) 5.5 g, (d) 5 g, and (e) 4 g.

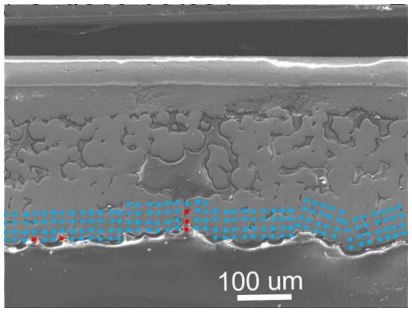

Figure 13 Cross-section of the microstructure of the half-cell with 4.5 g of pore former in the stainless steel sintered under an alumina plate lid at 1300 °C for 5 min.

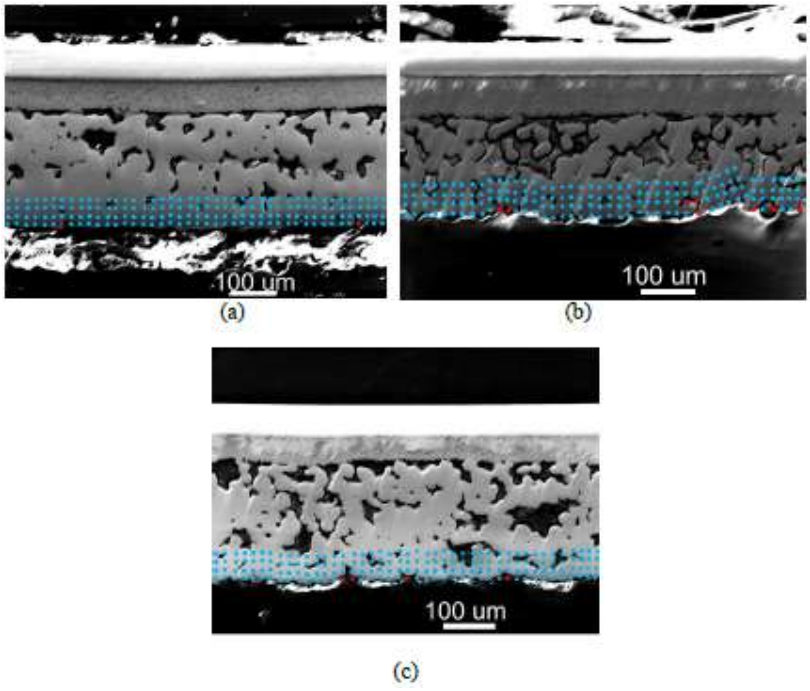

Figure 14 Cross-section microstructure of half-cells sintered at 1300 °C for 3 hours: (a) half-cell with 4 g pore former in the stainless steel sintered in open space, (b) containing 4 g pore former sintered with an alumina plate lid spaced by 2 mm, (c) containing 5.5 g pore former sintered in open space.

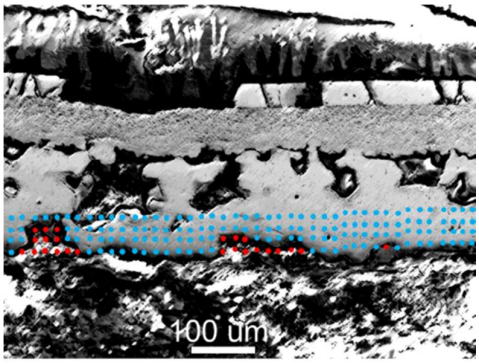

Figure 15 Cross-section of the microstructure of the half-cell with 3.7 g pore former in the stainless steel sintered in open space at 1300 °C for 5 hours. The image shows the tested cell that was broken after testing.

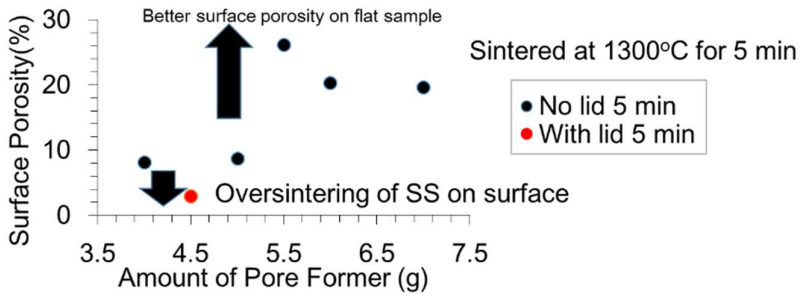

(a)

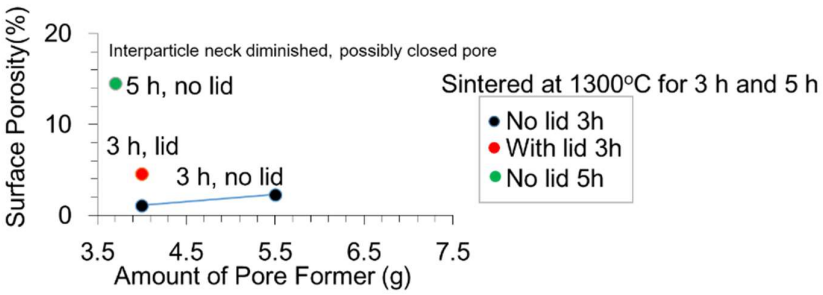

(b)

Figure 16 Stainless steel surface porosity vs amount of pore former in the stainless steel layer: (a) sintered at 1300 °C for 5 min and (b) sintered at 1300 °C for 3 h and 5 h.

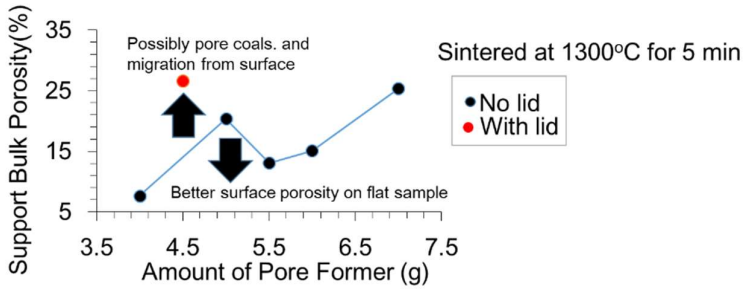

(a)

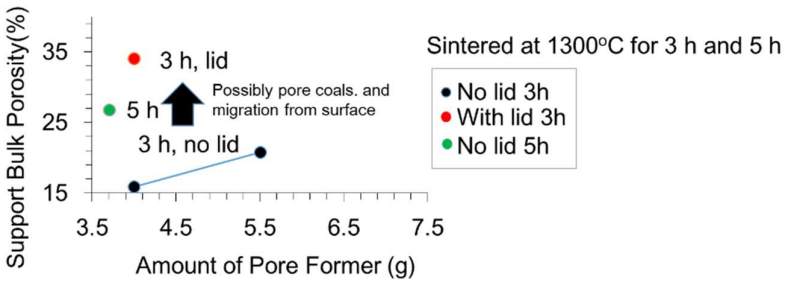

(b)

Figure 17 Stainless steel bulk porosity vs variation of the amount pore former added: (a) is for the half-cell sintered at 1300 °C for 5 minutes, and (b) is for the half-cell sintered at 1300 °C for 3 h and 5 h.

3.5 Residual Stresses

Table 4 shows the amount of residual stress measured on the half-cell surface of the stainless steel and the 8 mol% YSZ. The magnitude of error in the measurements of the stainless steel layer was so large because of machine limitations, where the grain or particle size has to be around 1 µm. Here, stainless steel powder with a particle size of around 40 µm was used. As for the magnitude of error in the measurements of the 8 mol% YSZ, it was sometimes below 50%, which shows its uncertainty. Considering a simple bilayer model of SS430L and 8YSZ without NiO-YSZ as interlayer, when SS430L dominates the shrinkage but is constrained by the 8YSZ (bilayer bent to steel), then the compressive residual stress on the 8YSZ will be retained, as shown in Figure 18. Ignoring the contribution of NiO-YSZ, the model displays the warpage behavior shown in Table IV in a fair amount of cases, where the sintered layers bent to 8YSZ cause tensile residual stress in the 8YSZ and vice versa.

Table 4 Residual stresses of sintered layers.

Holding time	Amount of pore former added (g)	Warpage behavior	Residual stress in 8 mol% YSZ (MPa)
5 min	7	Bent to steel	47 ± 12
5 min	6	Bent to steel	-46 ± 6
5 min	5.5	Slightly flat	-35 ± 6
5 min	5	Bent to 8YSZ	144 ± 130
5 min	4	Bent to 8YSZ	36 ± 15
5 min with lid	4.5	Slighly flat	-1 ± 10
3 h	4	Bent to 8YSZ	14 ± 7
3 h with lid	4	Slightly flat	-35 ± 8
3 h	5.5	Bent to steel	-115 ± 12
5 h	3.7	Slightly flat	-140 ± 7

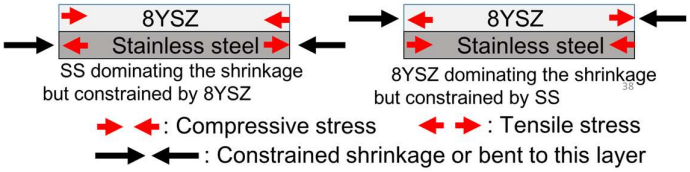

Figure 18 Bilayer of SS430L-8YSZ (without NiO-YSZ) and its residual stress evolution during sintering.

3.6 Cell Performance

Electrochemical tests were performed on the 5.5-g pore former sample sintered at 1300 °C for 5 minutes with humidified hydrogen as fuel and air as oxidant at 600, 650, and 700 °C. The cell voltages and power densities are shown in Figure 19. The open circuit voltage decreased from 1.025 V at 600 °C under 20%H_2/Ar-3%H_2O to 0.99 V at 700 °C under 10%H_2/Ar-3%H_2O and was within 50 mV of the theoretical cell OCPs, indicating excellent impermeability of the YSZ electrolyte, as shown in Figure 19. The I-V characteristic curve shown in Figure 19 was taken by sweeping the voltage from OCP to 0.4 V. The maximum power densities under 20%H_2/Ar-3%H_2O were 3, 5.2 and 9.5 mWcm^{-2} at 600, 650, 700 °C, respectively and the maximum power densities under 10%H_2/Ar-3%H_2O were 3, 5.2 and 10.8 mWcm^{-2} at 600, 650, 700 °C respectively. The current density was 0.015 A/cm^2 at 0.7 V and 700 °C under 10%H_2/Ar-3%H_2O, corresponding to a power density of 8.26 mWcm^{-2}. This value is still lower than previously reported power density values, for example by Villareal, *et al.* [2]. The OCPs showed that the electrolyte was impermeable, however, the maximum power density was so low that the microstructure of the cell needs to be improved,

for example by increasing the density of the electrolyte to optimize the microstructure of the anode and the stainless steel support.

The current-voltage curve in Figure 19 shows that the current magnitude curved back when more overpotential was given. It is thought that this phenomenon could be a sign of a degrading chemical reaction happening in one of the layers of the cell when more overpotential was given.

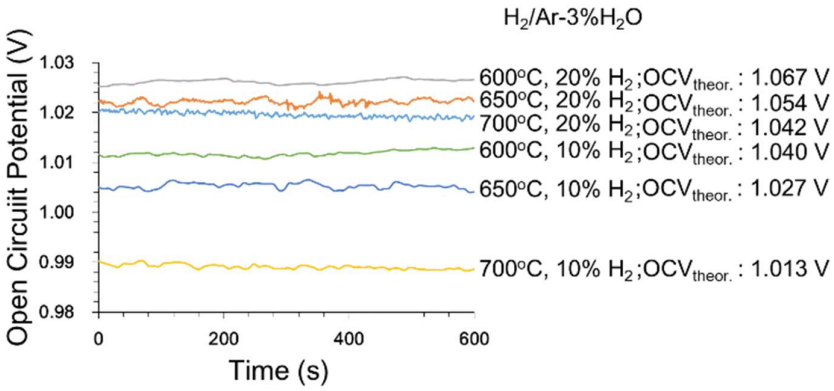

(a)

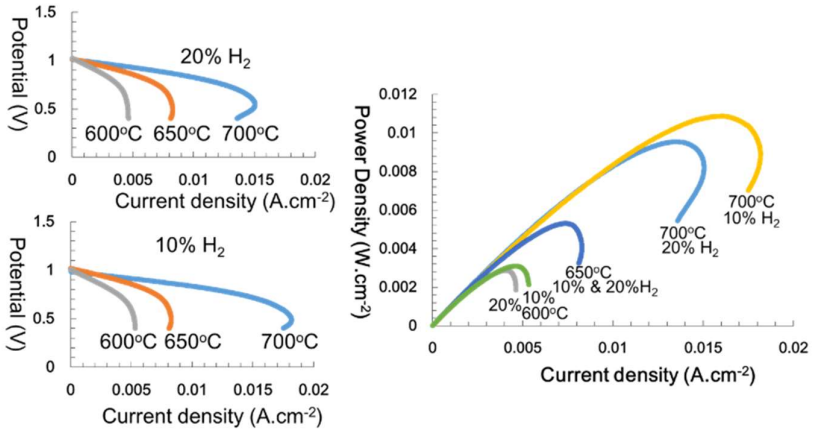

(b)

Figure 19 OCP curve vs time (a) and I-V characteristics of a single cell (b) sintered at 1300 °C for 5 minutes with 5.5 g of pore former in the stainless steel layer. The current steady state condition was not checked.

It can be seen that this chemical reaction was a thermally activated reaction, as it only occurred at higher operation temperature. A degrading reaction occurring at this higher temperature could be caused by reaction products building up in the dense oversintered anode, resulting in Nernst's loss following the Nernst equation for cell voltage. This Nernst loss can be explained as a loss in cell voltage due to a local increase of oxygen partial pressure in the anode. Nevertheless, after the sample was cooled down from testing operating condition, it was found that a crack had appeared in the 8YSZ layer. After further observation with a data logger, it was found that a leak had occurred several hours after the sample reached room temperature. From this it is thought that the observed crack may have propagated after room temperature was reached. This may be contributed to the mechanical sealing mechanism with vermiculite giving a considerable amount of pressure to the cell. Further improvement of the sealing mechanism is advised.

4 Conclusions

The effect of variation of the amount of pore former added to stainless steel slurry on the resulted half-cell flatness was studied. It was confirmed that the pore former amount added to the stainless steel affects the half-cell multilayer sintering behavior. By controlling the amount of pore former added to the stainless steel, flatness of the half-cell can be achieved. The effect of sintering time showed that the sinterability of the stainless steel in our work could be reduced by decreasing the amount of pore former. The grain size of the 8 mol% YSZ increased with increasing sintering time. The dihedral angle of the sintered stainless steel particles also increased with increasing sintering time. It was found that the stainless steel surface suffered from oversintering becoming larger as the sintering time was prolonged and the above sample was given a lid in order to homogenize the temperature. The half-cell with 5.5 g of pore former sintered at 1300 °C for 5 minutes had the best flatness and combination of stainless steel surface porosity and bulk porosity. Residual stress measurements were also done on the surface of the stainless steel layer and the 8 mol% YSZ. It was shown that the sintered metal-supported SOFCs bent to the electrolyte were associated with tensile stress in the electrolyte and vice versa for the SOFCs bent to the stainless steel support. A single cell with 5.5 g of pore former sintered at 1300 °C for 5 minutes with a silver paste cathode was able to produce 10 mW/cm^2 on 10% H_2/Ar-3%H_2O at 700 °C. This work hopes to contribute to the theoretical sintering process derivation for MS-SOFC fabrication.

Acknowledgement

This work was carried out as part of a project supported by the New Energy and Industrial Technology Development Organization (NEDO).

References

[1] Tucker, M., *Progress in Metal-supported Solid Oxide Fuel Cells: A Review,* Journal of Power Sources, **195**(15), pp. 4570-4582, 2010.

[2] Villarreal, I., Jacobson, C., Leming, A., Matus, Y., Visco, S. & De Jonghe, L., *Metal-supported Solid Oxide Fuel Cells*, Electrochemical and Solid-State Letters, **6**(9), pp. A178-A179, 2003.

[3] Zhou, Y., Ye, X., Li, J., Zhan, Z. & Wang, S., *Metal-supported Solid Oxide Fuel Cells with a Simple Structure*, Journal Electrochemical Society, **161**(9), pp. F332-F336, 2014.

[4] Hwang, C.S., Tsai, C.H., Yu, J.F., Chang, C.L., Lin, J.M., Shiu, Y.H. & Cheng, S.W., *High Performance Metal-supported Intermediate Temperature Solid Oxide Fuel Cells Fabricated by Atmospheric Plasma Spraying,* Journal of Power Sources, **196**(4), pp. 1932-1939, 2011.

[5] Ju, Y. W., Eto, H., Inagaki, T., Ida, S. & Ishihara, T., *Preparation of Ni–Fe Bimetallic Porous Anode Support for Solid Oxide Fuel Cells Using LaGaO3 based Electrolyte Film with High Power Density*, Journal of Power Sources, **196** (19), pp. 6294-6300, 2010.

[6] Franco, T. & Hoshiar Din, Z., *Ceramic Diffusion Barrier Layers for Metal Supported SOFCs,* ECS Transactions, **7**(1), pp. 771-780, 2007.

[7] M. Tucker. *Development of High Power Density Metal-supported Solid Oxide Fuel Cells*, Energy Technology, **5**(12), pp. 2175-2181, 2017.

[8] Zhou, Y., Zhang, Z., Yuan, C., Li, J., Xia, C., Zhan, Z. & Wang, S., *Metal Supported Solid Oxide Fuel Cells with In-situ Sintered (Bi_2O_3) 0.7 (Er_2O_3) 0.3–Ag Composite Cathode,* International Journal of Hydrogen Energy, **38**(36), pp. 16579-16583, 2013.

[9] Toor, S.Y., *High Temperature Co-Sintering for Metal Supported-Solid Oxide Fuel Cell Fabrication,* Doctoral dissertation: University of Waterloo, 2019.

[10] Green, D.J., *Constrained sintering: A Delicate Balance of Scales.* Journal of the European Ceramic Society, **28**(7), pp. 1451-1466, 2008.

[11] Roussel, D., Lichtner, A., Jauffrès, D., Villanova, J., Bordia, R. K. & Martin, C. L., *Strength of Hierarchically Porous Ceramics: Discrete simulations on X-ray Nanotomography Images*, Scripta Materialia, **113,** pp. 250-253, 2016.

[12] Liu, X., Martin, C.L., Delette, G., Laurencin, J., Bouvard D. & Delahaye, T., *Microstructure of Porous Composite Electrodes Generated by the Discrete Element Method,* Journal of Power Sources, **196** (4), pp. 2046-2054, 2011.

[13] Huang, R. & Pan, J., *A Further Report on Finite Element Analysis of Sintering Deformation Using Densification Data—Error Estimation and*

Constrained Sintering, Journal of the European Ceramic Society, **28**(10), pp. 1931-1939, 2008.

[14] Molla, T.T., Ni, D.W., Bulatova, R., Bjørk, R., Bahl, C., Pryds N. & Frandsen H.L., *Finite Element Modeling of Camber Evolution During Sintering of Bilayer Structures*, Journal of the American Ceramic Society, **97** (9), pp. 2965-2972, 2014.

[15] Bjørk, R., Frandsen H.L. & Pryds, N., *Modeling the Microstructural Evolution during Constrained Sintering,* Journal of the American Ceramic Society, **98**(11), pp. 3490-3495, 2015.

[16] Lu, J., Hng, H.H., Song, X., Zhang, T. & Ma, J., *Cosintering of a Bimodal Pore Distribution Layered Structure: Constitutive Models and Experiment,* Journal of the American Ceramic Society, **94**(5), pp. 1528-2535, 2011.